Solar Phys
DOI 10.1007/s11207-012-0164-9



# Scientific Analysis within SEPServer – New Perspectives in Solar Energetic Particle Research: The Case Study of the 13 July 2005 Event

**O.E. Malandraki · N. Agueda · A. Papaioannou · K.-L. Klein · E. Valtonen · B. Heber · W. Dröge · H. Aurass · A. Nindos · N. Vilmer · B. Sanahuja · A. Kouloumvakos · S. Braune · P. Preka-Papadema · K. Tziotziou · C. Hamadache · J. Kiener · V. Tatischeff · E. Riihonen · Y. Kartavykh · R. Rodríguez-Gasén · R. Vainio**

Received: 23 March 2012 / Accepted: 10 October 2012


**Abstract** Solar energetic particle (SEP) events are a key ingredient of solar–terrestrial physics both for fundamental research and space weather applications. Multi-satellite observations are an important and incompletely exploited tool for studying the acceleration and the coronal and interplanetary propagation of the particles. While STEREO uses for this diagnostic two identical sets of instrumentation, there are many earlier observations carried out with different spacecraft. It is the aim of the SEPServer project to make these data and analysis tools available to a broad user community. The consortium will carry out

The Sun 360
Guest Editors: Bernhard Fleck, Bernd Heber, and Angelos Vourlidas

O.E. Malandraki (✉) · A. Papaioannou · K. Tziotziou
Institute for Astronomy, Astrophysics, Space Applications and Remote Sensing, National Observatory of Athens, Athens, Greece
e-mail: omaland@astro.noa.gr

A. Papaioannou
e-mail: atpapaio@astro.noa.gr

N. Agueda · B. Sanahuja
Dept. d'Astronomia i Meteorologia and Institut de Ciéncies del Cosmos, Universitat de Barcelona, Barcelona, Spain

N. Agueda
e-mail: nagueda@am.ub.es

B. Sanahuja
e-mail: Blai.Sanahuja@ub.edu

K.-L. Klein · N. Vilmer · R. Rodríguez-Gasén
LESIA-Observatoire de Paris, CNRS, UPMC, Univ Paris 06, Univ. Paris-Diderot, Paris, France

K.-L. Klein
e-mail: ludwig.klein@obspm.fr

N. Vilmer
e-mail: nicole.vilmer@obspm.fr

R. Rodríguez-Gasén
e-mail: rosa.rodriguez@obspm.fr

Published online: 01 November 2012

data-driven analysis and simulation-based data analysis capable of deconvolving the effects of interplanetary transport and solar injection from SEP observations, and will compare the results with the electromagnetic signatures. The tools and results will be provided on the web server of the project in order to facilitate further analysis by the research community. This paper describes the data products and analysis strategies with one specific event, the case study of 13 July 2005. The release time of protons and electrons are derived using data-

E. Valtonen · E. Riihonen
Space Research Laboratory, Department of Physics and Astronomy, University of Turku, Turku, Finland

E. Valtonen
e-mail: Eino.Valtonen@utu.fi

E. Riihonen
e-mail: Esa.Riihonen@utu.fi

B. Heber
Christian-Albrechts-Universität zu Kiel, Kiel, Germany
e-mail: heber@physik.uni-kiel.de

W. Dröge · Y. Kartavykh
Julius-Maximilians Universität Würzburg, Würzburg, Germany

W. Dröge
e-mail: wolfgang.droege@astro.uni-wuerzburg.de

H. Aurass · S. Braune
Leibniz-Institut für Astrophysik Potsdam (AIP), Potsdam, Germany

H. Aurass
e-mail: haurass@aip.de

A. Nindos · A. Kouloumvakos
University of Ioannina, Ioannina, Greece

A. Nindos
e-mail: anindos@cc.uoi.gr

A. Kouloumvakos · P. Preka-Papadema
National and Kapodistrian University of Athens, Athens, Greece

P. Preka-Papadema
e-mail: ppreka@phys.uoa.gr

C. Hamadache · J. Kiener · V. Tatischeff · R. Rodríguez-Gasén
CSNSM, IN2P3-CNRS, Univ Paris-Sud, Paris, France

C. Hamadache
e-mail: clarisse.hamadache@csnsm.in2p3.fr

J. Kiener
e-mail: jurgen.kiener@csnsm.in2p3.fr

V. Tatischeff
e-mail: vincent.tatischeff@csnsm.in2p3.fr

Y. Kartavykh
Ioffe Physical-Technical Institute, St-Petersburg, Russia

R. Vainio
Department of Physics, POB64, 00014, University of Helsinki, Helsinki, Finland
e-mail: rami.vainio@helsinki.fi

driven and simulation-based analyses, and compared with hard X-ray and radio signatures. The interconnection of the experimental and the simulation-based results are discussed in detail.

**Keywords** Solar energetic particles · Coronal mass ejections · Interplanetary propagation · Monte Carlo simulation · Radio signatures

## 1. Introduction

### 1.1. Solar Energetic Particles

The acceleration mechanisms and transport processes of solar energetic particles (SEP) constitute up-to-date highly important scientific issues. SEP events and their transport through interplanetary (IP) space offer a unique opportunity to analyze their acceleration mechanisms and their sources while at the same time provide the testing of the energetic particles propagation theories through numerical simulations and comparisons with the *in-situ* measurements. SEP events originate by either solar flares or coronal mass ejections (CMEs) (Reames, 1999) and are frequently (but roughly) categorized as gradual or impulsive. The production of SEP events related to solar flares represents the outflow of particles during magnetic reconnection in active regions (Klein and Posner, 2005). SEP events are also produced by acceleration of particles at collisionless shock waves driven by CMEs (Reames, 1999, 2009). Shock-accelerated particles are injected into the heliosphere and propagate along interplanetary magnetic field (IMF) lines. When the magnetic connection between the observer and the field lines along which these particles propagate is established, particle flux enhancements are observed at the detectors in space (Heras *et al.*, 1992, 1995; Lario, Sanahuja, and Heras, 1998; Aran *et al.*, 2007).

Multipoint particle measurements are an important tool to understand the origin and propagation of SEP. They are one of the drivers of the STEREO concept (Kaiser *et al.*, 2008). However, many independent measurements from earlier spacecraft are available for exploitation. One limitation to their usefulness is that the data are not publicly available or, if they are, through instrument-specific access procedures and in different data formats. Advanced tools to interpret the data, including the analysis of particle propagation to the spacecraft, are only used by a few experts. There is furthermore a potential for the comparison of SEP measurements with electromagnetic signatures of particle acceleration at the Sun that is presently underexploited. Usually the access and handling of electromagnetic data are completely independent of SEP data. The SEPServer project aims at facilitating SEP analyses themselves and comparative studies of SEP and electromagnetic emission signatures by making the data and analysis tools available on a unique internet-based server. It will also include state-of the-art analysis tools based on numerical simulations on particle transport in the interplanetary medium (for more details of the SEPServer project, see Vainio *et al.*, 2012). In this work we present the case study of the 13 July 2005 SEP event which constitutes first collaborative results and demonstrates the new perspectives that will be made available to the future user of SEPServer.

## 2. Instrumentation and Data Description

### 2.1. SOHO/ERNE

The *Energetic and Relativistic Nuclei and Electron* (ERNE) experiment onboard the *Solar and Heliospheric Observatory* (SOHO) provides proton and heavy-ion data for the

SEPServer project. ERNE operates in the proton energy range of 1.5 – 140 MeV by using two sensors. For heavy ions the energy range extends up to $\sim$ 500 MeV/nucleon. Particle identification is based on the well-known delta E-E method. The *Low Energy Detector* (LED) is a simple stack of silicon detectors with the first detector layer divided into seven independent parts and covering a view cone with full opening angle of 64°. The *High Energy Detector* (HED) operates from 12 MeV upwards and has a field of view of 120°. Due to this wide field of view the path length variations of particles in the detectors have to be taken into account in order to preserve a good mass resolution. This is achieved by using silicon strip detectors measuring the angle of incidence of particles with an accuracy of $\sim 6°$. Thus, the strip detectors also allow detailed directional measurements of particles within the wide field of view of HED. Operational energy range of HED up to 140 MeV for protons is accomplished by using two layers of heavy scintillators (CsI(Tl) and BGO) stopping the particles. The geometric factor of LED is 0.915 $cm^2$ sr. In HED the geometric factor is strongly dependent on particle species and energy varying within 13 – 47 $cm^2$ sr. Since SOHO is a 3-axis stabilized spacecraft pointing to the center of the Sun, ERNE measurements are limited within the 64° and 120° fields of view around the instrument axes, which are pointed along the nominal interplanetary magnetic field direction, 45° to the west of the Sun. More detailed descriptions of the ERNE experiment can be found in Torsti *et al.* (1995) and Valtonen *et al.* (1997).

### 2.2. SOHO/EPHIN

The *Electron Proton and Helium Instrument* (EPHIN) onboard SOHO is part of the COSTEP (*Comprehensive Suprathermal and Energetic Particle Analyzer*) experiment that studies the suprathermal and energetic particle populations of solar, interplanetary, and galactic origin. The EPHIN sensor is a stack of six cylindrical solid state detectors surrounded by a plastic scintillator. The two first thinner detectors are divided in six sectors to allow a rough trajectory determination and particle range corrections, which improve isotopic discrimination (Müller-Mellin *et al.*, 1995). The sensor points along the nominal direction of the interplanetary magnetic field 45° west with respect to the spacecraft-Sun line. The maximum temporal resolution is 1 minute and the nominal geometric factor is 5.1 $cm^2$ sr.

### 2.3. ACE/EPAM

The *Electron Proton and Alpha Monitor* (EPAM) measures ions and electrons over a broad range of energy and intensity with five separate telescopes that provide nearly full coverage of the full sky in one spin period (Gold *et al.*, 1998). For the purposes of the current study high-resolution electron data obtained by two telescopes onboard EPAM, *i.e.* the *Low-Energy Magnetic Spectrometer* (LEMS30) and the *Low-Energy Foil Spectrometer* (LEFS60), have been used. The first telescope, LEMS30, registers electrons by the magnetic deflection of the incoming particles with energy below 315 keV into the detector. Thus the electrons measured in this technique are called deflected electrons (DEs). Deflected electrons are measured in four electron channels in the energy range 38 – 315 keV. LEMS30 sweeps out an annulus centered at 30° ($\pm$ 25°) to the sunward spin axis of ACE spacecraft (Stone *et al.*, 1998), and data are accumulated in four 90° sectors. The LEFS60 telescope registers electrons (E's) using a foil to absorb ions with energies below approximately 350 keV, while allowing electrons with energies $>$ 45 keV to pass through to the detector. LEFS60 measures electrons into four energy channels between 45 – 312 keV, while it samples an annulus centered at 60° ($\pm$ 25°) to the ACE spin axis, divided into eight 45° sectors.

### 2.4. *Wind*/3DP

The three-dimensional *Plasma and Energetic Particle Investigation* (3DP) is designed to make measurements of the full three-dimensional distribution of suprathermal electrons and ions from solar wind plasma to low energy cosmic rays, with high sensitivity, wide dynamic range, excellent energy and angular resolution, and high time resolution. Three arrays, each consisting of a pair of double-ended semi-conductor telescopes, measure electrons and ions above 20 keV. One side of each telescope is covered with a thin foil which absorbs ions below 400 keV, while on the other side the incoming $< 400$ keV electrons are swept away by a magnet, therefore electrons and ions are cleanly separated. Full sky coverage can be obtained in one spin (Lin *et al.*, 1995).

## 3. Data Analysis Methods

### 3.1. Onset Time Determination

Similar algorithms for both EPHIN and EPAM level 2 data have been developed, for the automatic determination of SEP event onset times at a given instrument channel. The basic concept of the algorithm, which aims to an objective criterion, is to compare the counts of the detector of a specified time window with the data just ahead of it. The main steps can be summarized as follows: Firstly, the algorithm determines the average intensity $\langle I \rangle$ and the standard deviation $\sigma$ inside the specified time window; next, it compares the data just ahead of this window with a threshold $\langle I \rangle + n \cdot \sigma$, where $n$ can be chosen by the user (typically $3 \cdot \sigma$ or $4 \cdot \sigma$ are used). When a number $m$ of consecutive points fulfils such condition ($m$ can be chosen by the user, typically set to $m = 2$ for EPHIN and $m = 4$ for EPAM), the onset is defined as the time stamp of the first point above the threshold.

If the condition is not fulfilled, the sampling window is moved one point forward in time and the process is repeated. In general the method is able to find onset times that match well the results obtained by human eye. In case of pre-event enhancements (*e.g.* events closely spaced in time or presence of X-ray contamination) the algorithm could fail to find the onset. Depending on the event conditions (poor statistics, very slow increase) longer time averages and different values of $n$ and/or $m$ could be required.

In order to determine the channel that will be used from the onset determination algorithm, one should take advantage of the fact that EPAM provides coverage of the full sky (see 2.3). This results into the identification of the anisotropic features of the electron recordings through the electron pitch-angle distributions (PADs). PADs from both LEFS60 and LEMS30 are used to pinpoint the sector of a specific detector that measures the particles more closely aligned to the IMF and therefore which system (LEMS30 or LEFS60) should be used to establish a precise electron onset time (Haggerty and Roelof, 2002). However, at this point it is important to note that LEFS60 is preferable as it provides much better angular coverage and has a larger geometrical factor. DEs and consequently LEMS30 are used only in case of significant ion contamination of E's during the onset time of the SEP.

Haggerty and Roelof (2002, 2003) used simulations to examine the effect of high-energy electrons which deposit only a fraction of the energy at the detector and thus are counted as low energy electrons. They concluded that while the effect can be significant in the lowest-energy channel (depending on the steepness of the incident electron spectrum) it is negligible in the highest two channels (E'3 and E'4) and consequently, those should be used in order to define the precise onsets of SEP events. In the current study, sectored recordings of E'4

(175 – 312 keV), the highest-energy channel, were used to reliably determine the onset of the events (see Section 4.1.2).

Onset time determination for SOHO/ERNE and *Wind*/3DP was done by using the so-called Poisson-CUSUM method (Huttunen-Heikinmaa, Valtonen, and Laitinen, 2005). This is analogous to a statistical quality control scheme deciding whether or not a process is in control, and if not, gives the exact moment of time when the failure happened. In this case, the failure is an SEP event causing intensities to rise above the pre-failure background. The updated algorithm used in this work allows changing background, which is often necessary to take into account, *e.g.*, SEP events preceding the one under investigation, when the background has not yet reached a constant quiet-time value. Other criteria used for event onset determination were described in Huttunen-Heikinmaa, Valtonen, and Laitinen (2005).

### 3.2. Velocity Dispersion Analysis

Velocity dispersion analysis (VDA) of an SEP event is based on determining the onset times of the event at various energies and presenting these onset times as function of inverse velocity of the particles at respective energies. The velocity dispersion equation at 1 AU can be written as

$$t_{\rm onset}(E) = t_0 + 8.33\frac{[\rm min]}{[\rm AU]} \cdot s \cdot \beta^{-1}(E), \tag{1}$$

where $t_{\rm onset}(E)$ is the observed onset time in min at particle kinetic energy $E$, $t_0$ is the release time (min) from the acceleration site, $s$ is the apparent path length (in AU) traveled by the particles, and $\beta^{-1}(E) = \frac{c}{v(E)}$ is the inverse velocity of the particles. Thus, by linear fitting of the onset times as a function of the corresponding inverse velocity, estimates for both the release time and the apparent path length of the particles can be obtained. We apply VDA for both SOHO/ERNE and *Wind*/3DP measurements.

## 4. Analysis of the 13 July 2005 SEP Event

Time evolution of both electron and proton profiles as observed by different instruments is presented in Figure 1. A series of successive SEP events starts on 13 July 2005 between 14:00 and 15:00 UT. In the following we analyze the first of these events.

### 4.1. Onset Time Determination by *In-situ* Measurements

#### *4.1.1. SOHO/ERNE and Wind/3DP*

ERNE proton data suffer from intermittency during large parts of the 13 July 2005 event making it difficult to determine accurate onset times at various energies. The intermittency is due to the operational mode of ERNE favoring heavy-ion data at the expense of protons. In this mode, protons are observed only during 4-minute intervals followed by 16 min in the "heavy-ion mode". Proton intensities during these 16 min are obtained by interpolation from averages before and after the interruption.

Proton intensities of the 13 July 2005 event show somewhat different characteristics depending on the energy range under inspection. In the MeV range the event occurs in the aftermath of a structured event starting early on 10 July 2005. At 2 MeV the onset time is before 19:00 UT with proton intensities rising with some fluctuations by almost two orders of magnitude reaching the maximum at around 04:00 UT on 14 July 2005.

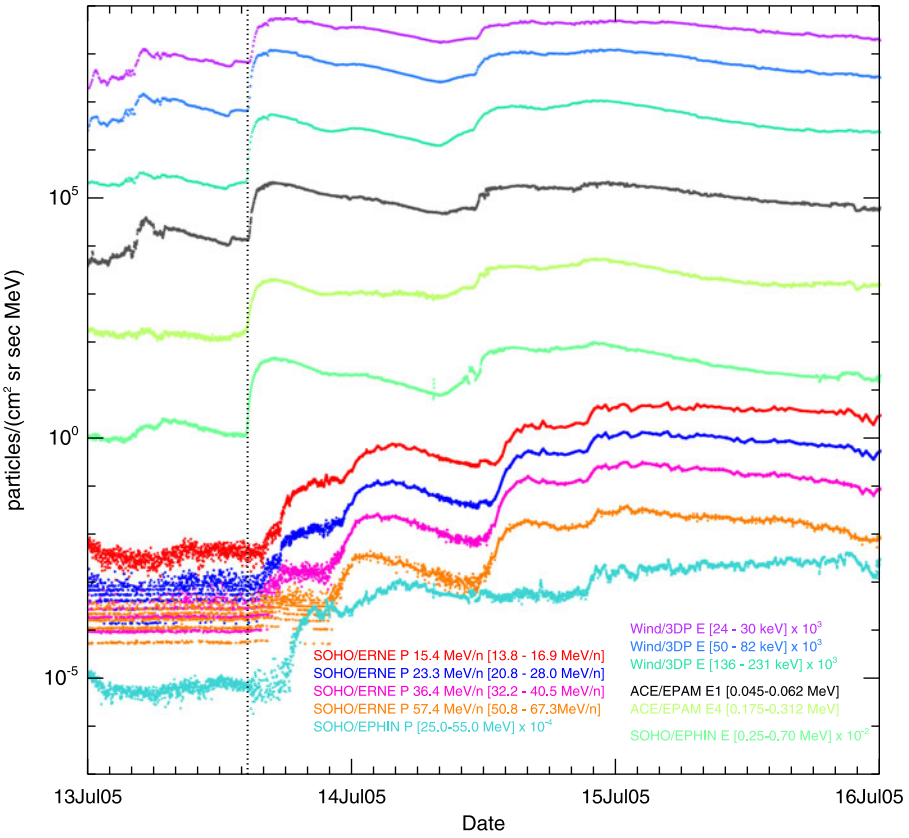


**Figure 1** Particle recordings from 13 to 16 July 2005. From top to bottom curves display: *Wind*/3DP electrons 24 – 231 keV in three energy ranges; ACE/EPAM electrons from 45 – 312 keV in two energy ranges; SOHO/EPHIN electrons from 0.25 – 0.70 MeV; SOHO/ERNE protons from 15.4 – 57.6 MeV/n in four energy ranges and SOHO/EPHIN protons from 25 to 55.0 MeV. A dashed line indicates the onset of the event at 14:30 UT, approximately.

In the 10-MeV range there are clearly two events on 13 July 2005 and a third one on 14 July 2005. The first event is obviously the one also seen at MeV-energies and for this event the VDA using the Poisson-CUSUM algorithm (see Section 3.2) at 17 energy channels (three highest energies discarded) gives the solar release time of 14:31 UT $\pm$ 15 min and the apparent path length of 2.84 $\pm$ 0.19 AU. The results of the VDA are presented in Figure 2 (left panel), where the onset time of the proton event observed in each energy channel as a function of the proton inverse velocity of the mean energy of each channel is shown. Due to the intermittency of ERNE data this algorithm does not necessarily give very accurate results. By inspecting the data by eye and determining the onset times in the same energy channels, the corresponding values of 14:40 UT $\pm$ 17 min and 2.32 $\pm$ 0.21 AU were obtained.

We have also used electron measurements by the SST telescope of the 3DP experiment on board the *Wind* spacecraft (Lin *et al.*, 1995) in the energy range 25 – 650 keV. We estimated the event onset time in each energy channel using the Poisson-CUSUM method (Huttunen-Heikinmaa, Valtonen, and Laitinen, 2005), as described in Section 3.2.

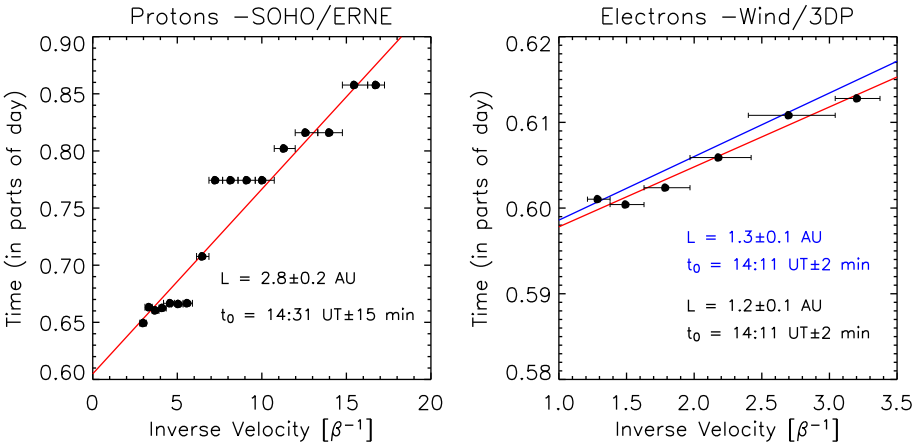


**Figure 2** Start times of the proton event observed by SOHO/ERNE (left panel) and the electron event observed by *Wind*/3DP (right panel), as a function of inverse velocity. Straight lines in both panels show a linear regression to the observations, where the slope corresponds to the apparent path length, and the intersection gives the solar release time for both protons and electrons. The blue line indicates VDA results by *Wind*/3DP taking the high-energy limit of the channels as a reference (see text for details).

Figure 2 (right panel) shows the onset time of the electron event observed in each energy channel as a function of the electron inverse velocity of the mean energy of each channel. Using a velocity dispersion analysis, we obtained an electron apparent path length $L = 1.2 \pm 0.1$ AU and a solar release time $t_0 = 14{:}11$ UT $\pm$ 2 min (14:19 UT if we add the 500 s for comparing to electromagnetic emissions). We performed a bootstrapping analysis to evaluate an error in the path length and the release time and we obtained $L = 1.2 \pm 0.2$ AU and a solar release time of 14:11 $\pm$ 2 min. When identifying the onset time of the event at the spacecraft we focus on the first signature of the electrons. Therefore we repeated the VDA analysis taking the high-energy limit of each channel as the reference. In this case, we obtained an electron apparent path length $L = 1.3 \pm 0.1$ AU and a solar release time $t_0 = 14{:}11$ UT $\pm$ 2 min ($L = 1.3 \pm 0.2$ AU and a solar release time of 14:11 $\pm$ 3 min, when bootstrapping). From the above investigation it is not unreasonable to suggest an IP path length between 1.2 and 1.3 AU, assuming that none of the measurements can be excluded from the VDA analysis.

### *4.1.2. SOHO/EPHIN and ACE/EPAM*

Concerning ACE/EPAM a comparison of the intensity profiles of electrons (from LEFS60) with the intensity profiles of the deflected electrons (from LEMS30) (not shown) reveals that the former follow closely the latter in structure during this period. Thus, it is concluded that LEFS60 response is primarily due to electrons. Given the fact that the geometrical factor of LEFS60 is larger than the LEMS30 one, the electron measurements from LEFS60 (E's) are used. Furthermore we note that this comparison also indicates that electron measurements from LEFS60 are considered clean (not contaminated by ions) during the initial phase of the SEP event and thus electron measurements from LEFS60 are ideal for the onset time determination.

Ten-minute averaged PADs for E'4 at 15:00 UT are embedded in Figure 3. Inspection of the PADs show that electrons do not exhibit strong anisotropic characteristics after the

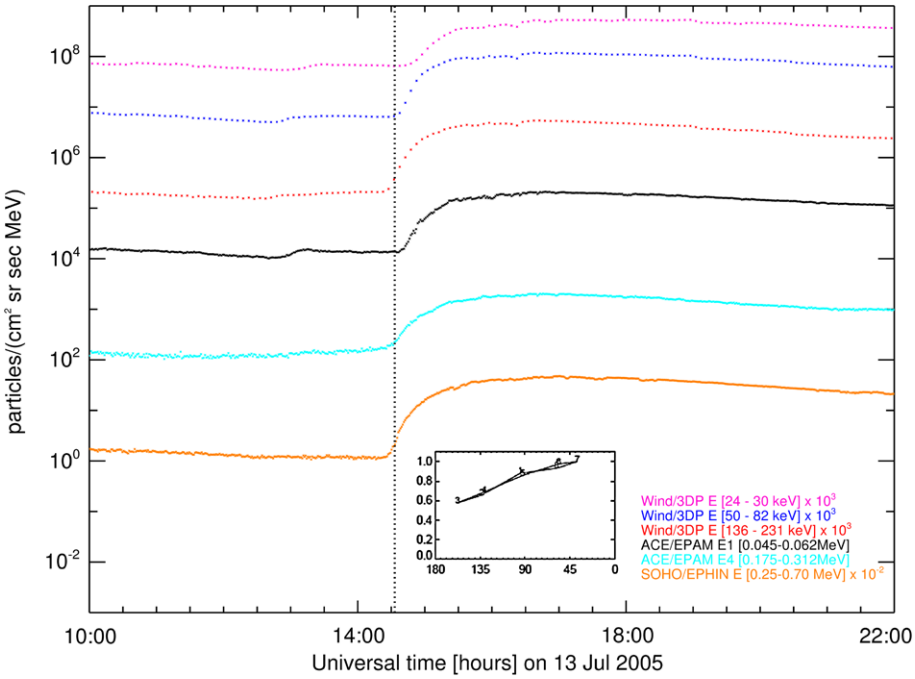


**Figure 3** Electron recordings from 13 to 14 July 2005 from *Wind*/3DP (24 – 231 keV in three energy ranges), ACE/EPAM (45 – 312 keV in two energy ranges) and SOHO/EPHIN (0.25 – 0.70 MeV). The dashed line represents the onset of the event at ∼ 14:30 UT. The embedded figure represents the pitch-angle distributions of ACE/EPAM high-energy electrons.

onset of the event, although the event is listed as a beam-like event.[1] Nevertheless, as can be inferred from Figure 3, sector 7 is being distinguished as the one along the magnetic field at the onset of the event. According to the method described in Section 3.1, we found that the 1-min high-energy electrons E'4 (175 – 312 keV) registered at sector 7, present an onset of the event at 14:33 UT. This result is in good agreement with the one presented at http://www.srl.caltech.edu/ACE/ASC/DATA/level3/.

The EPHIN intensity–time profiles of 0.25 to 0.7 MeV electrons are presented in Figure 3. Applying the onset time algorithm, described in Section 3.1, reveals an increase of the near-relativistic electrons at 14:27 UT.

The anticipated release time from ACE/EPAM measurements is based on the assumption that the velocity vector of the first arriving particles constitutes an angle of 0° with the vector of the magnetic field. Using the measured solar wind velocity of 600 km s$^{-1}$ by the SWEPAM experiment[2] (McComas *et al.*, 1998) on board ACE at the time of the onset of the electron event, the length of the Parker spiral connecting Earth to the Sun, was numerically calculated to be $L = 1.09$ AU (Malandraki *et al.*, 2002; Vainio *et al.*, 2012). We calculate the travel time of the E'4 high-energy electrons along the aforementioned path length to be 12.2 min. The corresponding release time (adding 500 s for direct comparison with 1-AU observations) is identified as 14:29 UT.

[1] http://www.srl.caltech.edu/ACE/ASC/DATA/level3/epam/BeamElectronEvents.pdf.

[2] http://www.srl.caltech.edu/ACE/ASC/level2/index.html.

### 4.2. Solar Observations

From the velocity dispersion analysis of the onset times of the SEP event solar release times of the electrons and protons were inferred near 14:00 – 14:30 UT (Section 3.2). Starting 12:54 UT, SOHO/LASCO observed a sequence of CMEs above the western solar limb. The brightest one was first seen at 14:30 UT above the occultation disk. SOHO/EIT observed eruptive activity in the underlying corona, including a system of rising loops that erupted between the images taken at 14:00 UT and 14:12 UT. This time interval marks the start and early rise of an M6.0 soft X-ray burst observed by GOES (Figure 4, bottom panel). This activity was accompanied by an Hα flare reported in *Solar Geophysical Data* (*Comprehensive Reports*) at N10W80 in active region NOAA 10786.

During this sequence of solar events, neither an interplanetary shock [3] nor an interplanetary coronal mass ejection[4] were registered. The origin of the SEP event under discussion must therefore be related to the dynamical processes in the corona related with the flare and CME near 14:00 UT. At this time the corona was perturbed by the previous CME, whose front was about 5 solar radii above the west limb near 14:00 UT. This may have some influence on particle transport.

The radio and hard X-ray emissions of this event were also discussed elsewhere (Battaglia and Benz, 2006; Chernov *et al.*, 2007; Krucker *et al.*, 2008; Caroubalos *et al.*, 2009). The time history of X-ray and radio emissions associated with the 13 July 2005 SEP event is shown in Figure 4. The panel displays, from bottom to top, the time profiles of soft X-ray and hard X-ray emissions, radio spectra and imaging observations. Hard X-ray data are provided from the *Anti-Coincidence Shield* (ACS) of the INTEGRAL hard X-ray and gamma-ray spectrometer and the *Ramaty High Energy Solar Spectroscopic Imager* (RHESSI) mission (Lin *et al.*, 2002). INTEGRAL/ACS was able to observe solar hard X-rays during the entire time interval plotted here (second panel from bottom), while RHESSI had many interruptions due to the occultation of the Sun by Earth, known as satellite night and the passage through the South-Atlantic Anomaly. Only the time profile observed during the second flare is shown here (red line). Dynamic radio spectra were provided by the ARTEMIS-IV spectrograph (Kontogeorgos *et al.*, 2006) in the range 20 – 650 MHz, the *Nançay Decameter Array* (Lecacheux, 2000) in the range 20 – 70 MHz and the WAVES spectrograph aboard the *Wind* spacecraft (Bougeret *et al.*, 1995) in the range 13.8 MHz – 20 kHz. The fourth and fifth panel from bottom show the spatial evolution of radio sources at 327 and 164 MHz observed by the *Nançay Radioheliograph* (Kerdraon and Delouis, 1997). Each 2D image is transformed into a 1D scan along the solar east–west axis by summing all pixels in the south–north direction. The field of view in these panels extends from the center of the solar disk to 2 $R_{\odot}$.

The plotted interval comprises two soft X-ray bursts (bottom panel). Both are associated with several intense type III bursts at decameter and longer wavelengths ($\nu \leq 70$ MHz; three top panels), which show that electron beams escape from the corona. The first soft X-ray burst (actually a superposition of two bursts) started near 12 UT and reached a peak flux $3 \times 10^{-5}$ W m$^{-2}$ (M3 class). INTEGRAL saw a short hard X-ray burst associated with the early phase of the soft X-ray burst. The type III bursts observed by ARTEMIS, NRH, NDA and WAVES, which show electron beams traveling through the corona and the interplanetary medium, clearly come later. The radio sources at meter waves were located at the western solar limb, as shown in Figure 4, where the projected distance from disk center is 1 $R_{\odot}$.

[3] http://www.ssg.sr.unh.edu/mag/ace/ACElists/obs_list.html#shocks.

[4] http://www.srl.caltech.edu/ACE/ASC/DATA/level3/icmetable2.htm.

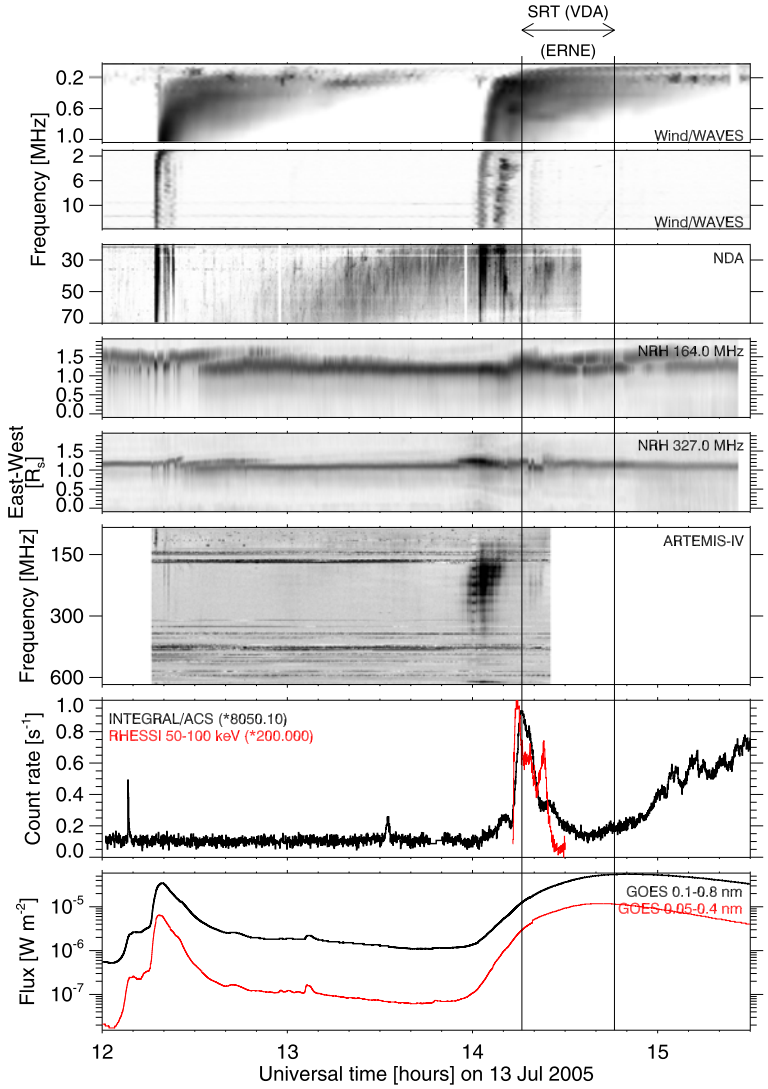


**Figure 4** Time history of radio and X-ray emission before and near the onset of the SEP event on 13 July 2005. From bottom to top: (i) soft X-ray flux in two wave bands (GOES satellites, NOAA), (ii) hard X-ray count rates in two photon energy ranges observed by the INTEGRAL/ACS and RHESSI instruments; (iii) radio spectrum at dm–m waves (ARTEMIS spectrograph); (iv) one-dimensional brightness, projected onto the solar east–west direction (*Nançay Radioheliograph*, NRH) between the center of the solar disk (0) and 2 $R_\odot$ west of it; (v) decameter-to-kilometer wave spectrum (*Nançay Decameter Array*, NDA, and *Wind*/WAVES radio spectrograph). Inverse color scale is used in the grey-scale plots (grey shading shows strong emission). The slow rise in the count rates of INTEGRAL/ACS starting near 14:40 UT is due to a contamination by energetic protons. The horizontal arrow above the plots and the two vertical dashed-dotted lines mark the time interval of solar proton release inferred from the velocity dispersion analyses of the SOHO/ERNE measurements.

A more conspicuous rise of the HXR emission started near 14 UT, up to a small peak, followed at 14:12 UT by the rise to the main peak. This burst was also detected by RHESSI. Its time profile was rather smooth as observed by INTEGRAL, but more structured into

bursts in the RHESSI records at lower photon energies. No relevant data exist in the minutes after 14:30 UT, when RHESSI was in the South Atlantic Anomaly, while INTEGRAL was hit by energetic ions that created the systematic rise seen until the end of the plotted time interval. Clearly the 14 UT soft X-ray burst was accompanied by efficient electron acceleration to tens and hundreds of keV in the low solar corona. But the relative timing of bright hard X-rays and metric and longer radio waves was unusual.

While the combination of soft and hard X-ray emissions with the type III bursts looks at first glance like a classical impulsive flare, the radio emissions from the middle corona (about $0.1-1\ R_{\odot}$ above the photosphere) show a more complex picture. The strongest emission (ARTEMIS, third panel from bottom) was a broad band type IV burst, which gradually drifted towards lower frequencies during the early rise of the second soft X-ray burst. It accompanied the first minor peak of hard X-ray emission and the most intense DH type III bursts. The NRH (panels 4 and 5 from bottom in Figure 4) observations show that this burst was part of a long-lasting emission, which actually started near 12:30 UT during the first soft X-ray burst. Different sources are apparent in the 1D plots. The source split in two during the 14 UT burst, with one source moving westward (moving type IV burst). This shows that different magnetic structures were involved in the emission, probably related to the early evolution of the CME. A counterpart of this long-lasting dm–m wave type IV burst is the diffuse drifting emitting feature observed by NDA from 13 UT onward at frequencies below 70 MHz. This emission exists at m and dm wavelengths, as shown by NRH, but is hidden within the background of the ARTEMIS spectrograph.

The dm–m-wave radio emissions suggest a connection between the two flares. The brightest part of the type IV burst near 14 UT displays an unusual timing with respect to the X-ray emission. Type IV bursts are generally found during the gradual phase of flares, near and after the maximum of the SXR burst. Here, however, the type IV emission occurred in the early impulsive phase, and before the strongest HXR emission. This timing suggests that the 14 UT burst was not a new event independent of the first, near 12 UT. Comparison of radio maps taken by NRH with EUV images from SoHO/EIT (not shown here) show that the radio sources are located in the vicinity of a system of EUV loops, which gradually rose from the first flare until 14:00 UT, and appeared disrupted in the following image (14:12 UT). It is tempting to relate the timing and location of the type IV emission to the evolution of these loops. Since the type IV burst occurred together with DH type III emission, it is closely related to the acceleration of electrons that escape to interplanetary space. This episode seems to precede the strongest hard X-ray emission. We cannot exclude that the main HXR peak was also associated with the release of electrons to interplanetary space, because the WAVES spectrum does show a faint third type III burst at that time. The velocity dispersion analysis of protons led to a later solar release, indicated by the vertical dashed-dotted lines in Figure 4. The bulk of HXR emission falls into this interval. As has been shown by earlier work, the injection time delays with respect to the impulsive flare phase are well possible during complex events (Aurass *et al.*, 2006).

So the electromagnetic emissions show that the solar release of SEP occurred during a complex sequence of acceleration episodes in the corona, related both to flaring activity and to the evolution of the magnetic environment over time scales from tens of minutes to several hours.

## 5. Modeling of Electron Transport and Injection

We modeled the 13 July 2005 electron event observed by the three-dimensional plasma and energetic particle (3DP) experiment on board the *Wind* spacecraft (Lin *et al.*, 1995), making

use of simulations of the interplanetary transport of solar energetic particles, followed by optimization of injection and transport parameters. In this section we compare three sets of simulation and fitting techniques.

### 5.1. Interplanetary Transport Models

In the absence of large-scale disturbances such as coronal mass ejections (CMEs) and shocks, the interplanetary magnetic field (IMF) can be described as a smooth average field, represented by an Archimedean spiral, with a superposed turbulent component. In this case, the propagation of charged particles along the IMF has two components, adiabatic motion along the smooth field and pitch-angle scattering by magnetic turbulence.

The quantitative treatment of the evolution of the particles' phase space density, $f(z, \mu, t)$, can be described by the focused transport equation (Roelof, 1969):

$$\frac{\partial f}{\partial t} + v\mu\frac{\partial f}{\partial z} + \frac{1-\mu^2}{2L}v\frac{\partial f}{\partial \mu} - \frac{\partial}{\partial \mu}\left(D_{\mu\mu}\frac{\partial f}{\partial \mu}\right) = q(z, \mu, t). \tag{2}$$

Here $z$ is the distance along the magnetic field line, $\mu$ is the particle pitch-angle cosine, and $t$ is the time. The systematic force is characterized by the focusing length, $L(z) = -B(z)/(\partial B/\partial z)$, in the diverging magnetic field $B$, while the stochastic forces are described by the pitch-angle diffusion coefficient $D_{\mu\mu}(\mu)$. The injection of particles close to the Sun is given by $q(z, \mu, t)$. This simple form of the equation neglects convection and adiabatic deceleration (see Ruffolo, 1995, for the full equation), but at the electron energies of interest in this paper, this is typically a small effect. Also we neglect here the effects of diffusion perpendicular to the average magnetic field (*e.g.*, Dröge *et al.*, 2010). Instead, it is assumed that there is no variation across the magnetic field, and that the respective solutions are identical in neighboring flux tubes.

Numerical methods are applied to solve Equation (2). Since early 1980s, finite-differences (FD) have been used for this purpose. Also, more recently, Monte Carlo (MC) simulations were employed to solve the corresponding stochastic differential equations (SDE).

In this work we use three different techniques to model the particle transport: a FD model (Dröge, 2003) that solves Equation (2) at a fixed particle energy, but has the advantage of being fast ($\sim$ one minute for one run), and two MC models (Kartavykh *et al.*, 2007; Agueda *et al.*, 2008) to solve the corresponding SDEs for an energy range adjusted to the width of the instrument channel under consideration. As usual, these models assume an Archimedean spiral magnetic flux tube connecting the Sun and the spacecraft, consistent with the solar wind speed measured *in situ*. As initial condition, electrons are released close to the Sun (at 10 and 2 solar radii, respectively), following a power law in energy in the MC models. The results of the models are intensity directional distributions of electrons at the spacecraft location resulting from an instantaneous injection close to the Sun, *i.e.*, they provide the Green functions of interplanetary transport.

The "standard model" (Jokipii, 1966; Jaekel and Schlickeiser, 1992) of particle scattering predicts a pitch-angle diffusion coefficient of the form $D_{\mu\mu} = \frac{1}{2}\nu(\mu)(1-\mu^2)$, where $\nu$ is the scattering frequency $\nu(\mu) = \nu_0|\mu|^{q-1}$, and $q$ is the spectral slope of the magnetic field power spectrum. For practical purposes often a pitch-angle diffusion coefficient of the form

$$D_{\mu\mu} = \frac{\nu_0}{2}\left(|\mu|^{q-1} + H\right)\left(1-\mu^2\right) \tag{3}$$

is assumed (Beek and Wibberenz, 1986), which partially resembles the result of the standard theory and additionally introduces a parameter $H$ to phenomenologically describe an enhancement of scattering through $\mu = 0$ by non-resonant and nonlinear effects. It is also possible to use a special dependence of $\nu(\mu)$ that resembles Equation (3), for example by assuming a scattering frequency of the form $\nu(\mu) = \nu_0(\frac{|\mu|}{1+|\mu|} + \epsilon)$, where $\epsilon$ is a parameter that allows us to consider a range of scattering conditions (Agueda *et al.*, 2008). For a number of parameters, the two models can be shown to be almost equivalent, for example they give very similar results for $(q, H) = (1.67, 0.05)$ and $\epsilon = 0.045$.

Under strong scattering conditions, the relation of $D_{\mu\mu}$ to the parallel scattering mean free path, $\lambda_\parallel$, is given by (Hasselmann and Wibberenz, 1970)

$$\lambda_\parallel = \frac{3v}{8} \int_{-1}^{1} \frac{(1-\mu^2)^2}{D_{\mu\mu}} \, \mathrm{d}\mu = \frac{3v}{4} \int_{-1}^{1} \frac{1-\mu^2}{\nu(\mu)} \, \mathrm{d}\mu. \tag{4}$$

However the mean free path has proved to be a convenient parameter to characterize the degrees of scattering even when the transport process cannot be considered as spatial diffusion because $\lambda_\parallel$ adopts values close to or larger than the observer's distance from the Sun. Following previous work (*e.g.* Palmer, 1982; Kallenrode, Wibberenz, and Hucke, 1992), we take the electron radial mean free path, $\lambda_r$, to be spatially constant. Then the mean free path parallel to the IMF line is given by $\lambda_\parallel = \lambda_r \sec^2 \psi$, where $\psi$ is the angle between the field line and the radial direction.

### 5.2. Fitting Techniques

Solutions of the transport equation have been widely used to model *in-situ* observations of SEP events with the goal of deriving the injection function and the interplanetary transport parameters. To this end, it is important to make use of the directional information contained in the data to be able to untangle the injection history and the transport scenario of the SEP events observed *in situ* (*e.g.* Agueda *et al.*, 2009b).

From a mathematical point of view, intensities measured at the spacecraft position can be seen as the "response" of the transport process, that is, as a result of a convolution between the Green function of interplanetary transport and the particle injection function (Ruffolo, Khumlumlert, and Youngdee, 1998). Thus, in principle, one can determine from *in-situ* data the transport conditions and the injection function close to the Sun by two approaches. One approach consists of assuming a parametrized injection function and finding the best fit by varying the injection and transport parameters. Another approach consists of tackling the inversion problem by solving a least-square problem with the constraint that the injection must be a non-negative function (see Agueda *et al.*, 2008 for more details). Finally, the set of "best fit" parameters can be found either "by eye" (*e.g.* Dröge and Kartavykh, 2009) or by an automated procedure that uses an estimator of the goodness of the fit (*e.g.* Maia *et al.*, 2007; Agueda *et al.*, 2008).

In this section, we compare several fitting techniques employing two different sets of data (omnidirectional intensities and first order anisotropies versus pitch-angle distributions) and two fitting methodologies (convolution and eye-ball fit versus inversion and goodness-of-fit estimator).

We use 50 – 82 keV electron measurements by *Wind*/3DP. The 3DP experiment uses several telescopes to cover the full sky in one spacecraft spin period, which allows a complete scan of the particle angular distribution. Pitch-angle distributions by *Wind*/3DP are normally provided with a pitch-angle resolution of 22.5° and they allow the omnidirectional intensity- and anisotropy-time profiles to be calculated for a given event.

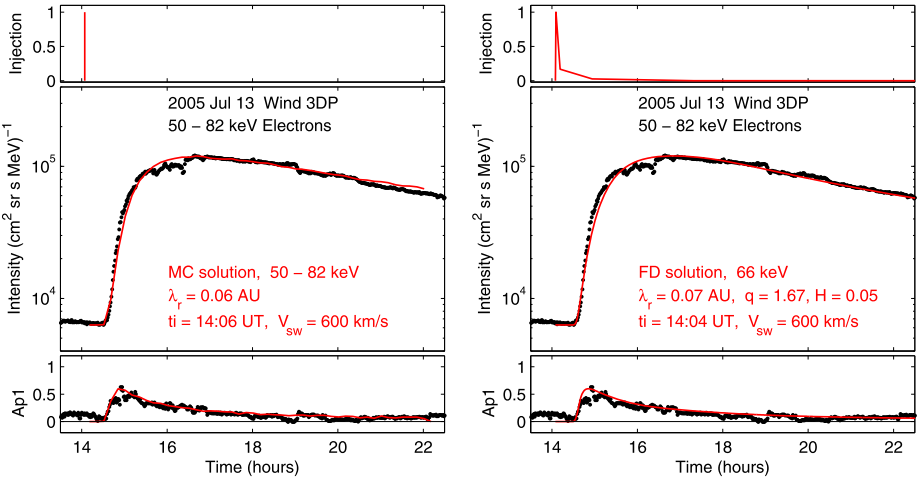


**Figure 5** Fits to the omnidirectional intensity–time and anisotropy–time profiles of 50 – 82 keV electrons observed by *Wind*/3DP on 13 July 2005. Left panel: MC solution for 50 – 82 keV electrons. Right panel: FD solution for 66 keV electrons. For each model, the top panel shows the derived injection function.

Figure 5 shows the omnidirectional intensity- and anisotropy-time profiles observed by *Wind*/3DP on 13 July 2005. The two panels show two different fits, both obtained by the "eye-ball"-fit method. In one case, the solutions of a MC transport model in the 50 – 82 keV energy range are used (left panel), while in the other a FD model is employed to solve the transport equation at the fixed energy of 66 keV. In both cases, the omnidirectional intensity and the first order anisotropy were tried to be simultaneously fit by means of varying the injection parametrization and the interplanetary transport conditions.

The transport parameters obtained from the two fits are very similar: $\lambda_r = 0.06$ AU for the MC model, and $\lambda_r = 0.07$ AU for the FD model. An instantaneous injection at 14:06 UT is deduced using the MC model, while a slightly longer injection is deduced from the FD model (see upper panels in Figure 5) starting at 14:04 UT. These differences possibly reflect the fact that the spread of electron energies (and resulting speeds) in the finite energy range of the MC model had to be mimicked by a spread in injection times in the fixed energy FD model for a similarly good fit. Therefore, the prediction of the MC model regarding the injection profile might be more realistic.

Figure 6 shows 50 – 82 keV electron intensities at eight different pitch-angles observed by *Wind*/3DP on 13 July 2005. Using solutions of a MC transport model in the 50 – 82 keV energy range and an inversion fitting approach together with an automated estimation of the goodness of the fit, we found that the best fit radial mean free path is $\lambda_r = 0.06$ AU. The injection profile for $\lambda_r = 0.06$ AU shows a prompt injection episode from 13:57 to 14:08 UT (peaking at 14:06 UT) that represents the 78 % of the whole injection. Another short and small injection episode starting around 15:18 UT is inferred from the fit. Figure 7 shows the inferred injection profile together with some of the electromagnetic emissions associated with the electron event. A comparison of timing indicates that the solar source is reasonably well represented by the type III radio burst, at energies 50 – 82 keV.

We performed a similar analysis for the 62 – 102 keV electron event observed by the EPAM experiment on board ACE (Gold *et al.*, 1998). We made use of the intensities measured by the LEFS60 telescope in eight different sectors. By taking the angular response

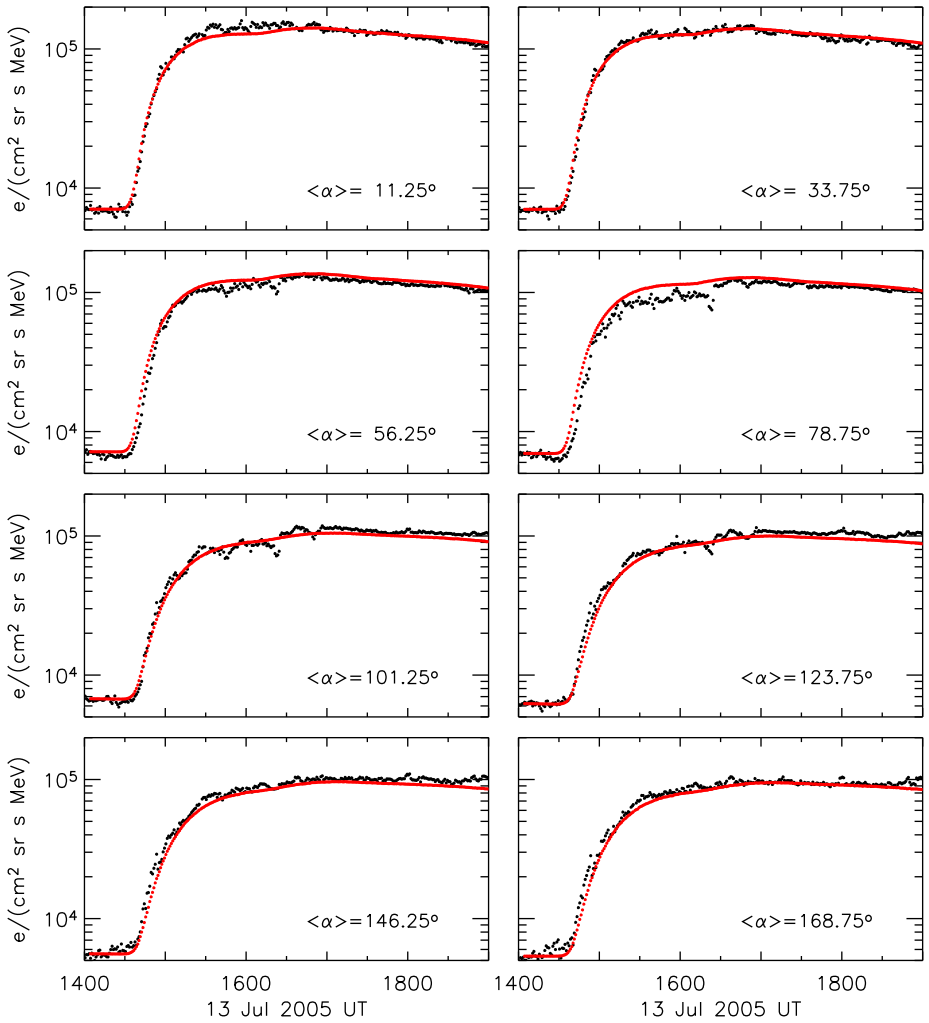


**Figure 6** Electron 50 – 82 keV intensities at eight different pitch-angles observed by *Wind*/3DP on 13 July 2005 (black dots). Each panel shows the time-intensity profiles in a pitch-angle ($\alpha$) bin with a resolution of 22.5°. The red curves show the modeled intensities inferred using an inversion fitting approach (see text for details) and assuming $\epsilon = 0.01$.

of each sector into account, the simulated Green functions were transformed into sectored Green's functions that allowed us to invert the observations (see Agueda *et al.*, 2009a for details). We obtained the best fit for $\lambda_r = 0.055$ AU and the injection profile was consistent with the timing and values inferred from the *Wind* observations (results not shown here).

We conclude that under similar assumptions, the values of the radial mean free path inferred either by eye-fitting the omnidirectional intensity and the first order anisotropy or by directly inverting the pitch-angle distributions do agree. Moreover, the injection profile deduced from a convolution approach agrees with the results obtained by using the automated inversion fitting technique.

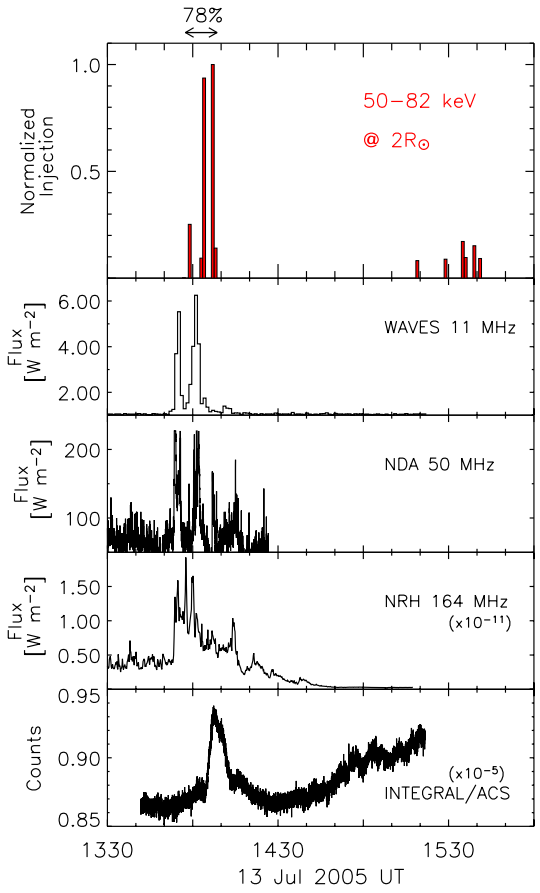


**Figure 7** From top to bottom: Normalized electron injection profile (red histogram) inferred from *Wind*/3DP observations using an inversion approach; light curves from WAVES (11 MHz), NDA (50 MHz), NRH (164 MHz) and INTEGRAL/ACS shifted − 500 s (light travel time to 1 AU) for direct comparison with the injection profile.

## 6. Discussion and Conclusions

In this work a case study of the 13 July 2005 event has been carried out using data from a large variety of instruments provided by the SEPServer project. Based on the observations by the SOHO/ERNE, SOHO/EPHIN, ACE/EPAM and *Wind*/3DP instruments it is evident that the event is clearly detected over an extensive energy range of 0.024 – 3.00 MeV for electrons and 7.8 – 57.6 MeV for protons (Figure 1). The VDA analysis of the high-energy proton and the near-relativistic electron measurements as provided by the SOHO/ERNE and the *Wind*/3DP instruments respectively, revealed a long apparent path length for protons, equal to 2.84 AU, whereas a shorter one was derived for electrons (1.2 AU, Table 1). The solar release times of the first near-relativistic electrons are inferred to occur 20 min before the energetic protons. We cannot say, based on one event study, if the difference of early release times of protons and electrons is a significant and systematic feature. However, we point out that *Helios* studies from the inner heliosphere did show different early release times of energetic electrons and protons (Kallenrode and Wibberenz, 1991) and that Krucker and Lin (2000) reported occasional findings where different path lengths were inferred from VDA for near-relativistic electrons and for protons at MeV energies. The SEPServer project aims at providing the data and tools necessary for comprehensive studies, using multiple spacecraft and complementary methods of analysis including interplanetary propagation.

**Table 1** Observational onset times from EPHIN and EPAM (e) and anticipated release time from ERNE (p) and 3DP (e).

| Instrument/ Species | Energy (MeV) | Onset time (UT) | Path length (AU) | Release time (UT) |
|---|---|---|---|---|
| ERNE (p) | 1.58 – 67.3 | | 2.84 | 14:31 ± 15 |
| | 1.58 – 67.3 | | 2.32 | 14:40 ± 17 |
| EPHIN (e) | 0.25 – 0.70 | 14:27 | 1.09 | |
| EPAM (e) | 0.175 – 0.312 | 14:33 | 1.09 | |
| 3DP (e) | 0.025 – 0.65 | | 1.2 | 14:11 ± 2 |

Inspection of the calculated electron pitch-angle distributions, as measured by the ACE/EPAM instrument, revealed that moderate anisotropic characteristics are observed after the onset of the event, which strongly implies scattering of the energetic particles in the IP space. The onset time of the event using SOHO/EPHIN and ACE/EPAM measurements has been determined and found to be at ∼ 14:30 UT for the electrons. The corresponding onset time for *Wind*/3DP 231 – 394 keV electrons, is 14:25 UT, therefore comparable, within errors, to the ones derived by SOHO/EPHIN and ACE/EPAM. The VDA analysis of *Wind*/3DP electrons provided a solar release time of 14:19 UT (adding 500 s for comparison reasons) and it is in good agreement with the associated EM solar emissions observations (Section 4.2) which showed that intense type III radio bursts, denoting solar electron release into open IMF field lines, occur from 14:00 UT onwards.

Using a different analysis perspective, the electron observations by both *Wind*/3DP and ACE/EPAM have been modeled during this event. Based on the fitting of the intensity and anisotropy time profiles observed, short mean free paths were derived for the electrons, denoting that those experienced significant scattering. This is in agreement with the observed pitch-angle distributions from ACE/EPAM which showed moderately anisotropic characteristics. Furthermore, the long apparent path length of protons obtained through the SOHO/ERNE VDA is consistent with a highly turbulent IP medium (Lintunen and Vainio, 2004; Saiz *et al.*, 2005). Note, however, the *Wind*/3DP VDA result for the path length (1.2 AU) seems too short for propagation in a turbulent medium. The results of *Wind*/3DP VDA may be somewhat compromised by the delayed onset of the highest-energy channel and the early onset of the lowest-energy channel (see Figure 2, right panel). Dropping these channels from the VDA would give a path length of 1.5 AU and the solar release time of 14:05 UT, which are already more consistent with the simulation results. This highlights the fact that VDA results cannot be trusted blindly but need to be taken with some precaution. It is noteworthy that the testing of the VDA method serves as an example of the systematic studies that will be enabled through SEPServer. The main result of the simulation analysis is that during this SEP event several impulsive injections take place, in close association with the aforementioned DH type III radio bursts starting at 14:00 UT and persistently observed afterwards, with the first prompt electron injection episode lasting from 13:57 – 14:08 UT (14:05 – 14:16 UT if we add 500 s for comparing to the EM emissions) representing the ∼ 78 % of the total injected particle population. The latter result is also in a reasonable good agreement with the results of the data-driven analysis which presents a coherent timing of the 13 July 2005 event.

The case study of the 13 July 2005 SEP event that has been analyzed in detail in the current work, is an illustration of the overall information that SEPServer will include and at the same time demonstrates the capabilities offered to its future users.

**Acknowledgements** The research leading to these results has received funding from the European Union's Seventh Framework Programme (FP7/2007-2013) under grant agreement No 262773 (SEPServer). NA and

BS also acknowledge financial support through the Spanish project AYA2010-17286, from the Ministerio de Ciencia e Innovacion, as well as the computational support provided by the Centre de Serveis Cientifics i Academics de Catalunya (CESCA).

## References

Agueda, N., Vainio, R., Lario, D., Sanahuja, B.: 2008, *Astrophys. J.* **675**, 1601.
Agueda, N., Vainio, R., Lario, D., Sanahuja, B., Kilpua, E., Pohjolainen, S.: 2009a, *Astron. Astrophys.* **507**, 981.
Agueda, N., Vainio, R., Lario, D., Sanahuja, B.: 2009b, *Adv. Space Res.* **44**, 794.
Aran, A., Lario, D., Sanahuja, B., Marsden, R.G., Dryer, M., Fry, C.D., McKenna-Lawlor, S.M.P.: 2007, *Astron. Astrophys.* **469**, 1123.
Aurass, H., Mann, G., Rausche, G., Warmuth, A.: 2006, *Astron. Astrophys.* **457**, 681.
Battaglia, M., Benz, A.O.: 2006, *Astron. Astrophys.* **456**, 751.
Beek, J., Wibberenz, G.: 1986, *Astrophys. J.* **311**, 437.
Bougeret, J.-L., Kaiser, M.L., Kellogg, P.J., Manning, R., Goetz, K., Monson, S.J., Monge, N., Friel, L., Meetre, C.A., Perche, C., Sitruk, L., Hoang, S.: 1995, *Space Sci. Rev.* **71**, 231.
Caroubalos, C., Preka-Papadema, P., Mavromichalaki, H., Moussas, X., Papaioannou, A., Mitsakou, E., Hillaris, A.: 2009, *Adv. Space Res.* **43**, 600.
Chernov, G.P., Kaiser, M.L., Bougeret, J.-L., Fomichev, V.V., Gorguts, R.V.: 2007, *Solar Phys.* **241**, 145.
Dröge, W.: 2003, *Astrophys. J.* **589**, 1027.
Dröge, W., Kartavykh, Y.: 2009, *Astrophys. J.* **693**, 69.
Dröge, W., Kartavykh, Y., Klecker, B., Kovaltsov, G.A.: 2010, *Astrophys. J.* **709**, 912.
Gold, R.E., Krimigis, S.M., Hawkins, S.E., Haggerty, D.K., Lohr, D.A., Fiore, E., Armstrong, T.P., Holland, G., Lanzerotti, L.J.: 1998, *Space Sci. Rev.* **86**, 541.
Haggerty, D.K., Roelof, E.C.: 2002, *Astrophys. J.* **579**, 841.
Haggerty, D.K., Roelof, E.C.: 2003, *Adv. Space Res.* **4**, 423.
Hasselmann, K., Wibberenz, G.: 1970, *Astrophys. J.* **162**, 1049.
Heras, A.M., Sanahuja, B., Smith, Z.K., Detman, T., Dryer, M.: 1992, *Astrophys. J.* **391**, 359.
Heras, A.M., Sanahuja, B., Lario, D., Smith, Z.K., Detman, T., Dryer, M.: 1995, *Astrophys. J.* **445**, 497.
Huttunen-Heikinmaa, K., Valtonen, E., Laitinen, T.: 2005, *Astron. Astrophys.* **442**, 673.
Jaekel, U., Schlickeiser, R.: 1992, *Ann. Geophys.* **10**, 541.
Jokipii, J.R.: 1966, *Astrophys. J.* **146**, 480.
Kaiser, M.L., Kucera, T.A., Davila, J.M., St. Cyr, O.C., Guhathakurta, M., Christian, E.: 2008, *Space Sci. Rev.* **136**, 5.
Kallenrode, M.-B., Wibberenz, G.: 1991, *Astrophys. J.* **376**, 787.
Kallenrode, M.-B., Wibberenz, G., Hucke, S.: 1992, *Astrophys. J.* **394**, 351.
Kartavykh, Y.Y., Dröge, W., Klecker, B., Mason, G.M., Möbius, E., Popecki, M., Krucker, S.: 2007, *Astrophys. J.* **671**, 947.
Kerdraon, A., Delouis, J.-M.: 1997, In: Trottet, G. (ed.) *Coronal Physics from Radio and Space Observations*, *Lecture Notes in Physics* **483**, 192.
Klein, K.-L., Posner, A.: 2005, *Astron. Astrophys.* **438**, 1029.
Kontogeorgos, A., Tsitsipis, P., Caroubalos, C., Moussas, X., Preka-Papadema, P., Hilaris, A., Petoussis, V., Bouratzis, C., Bougeret, J.-L., Alissandrakis, C.E., Dumas, G.: 2006, *Exp. Astron.* **21**, 41.
Krucker, S., Lin, R.P.: 2000, *Astrophys. J. Lett.* **542**, L61.
Krucker, S., Battaglia, M., Cargill, P.J., Fletcher, L., Hudson, H.S., MacKinnon, A.L., Masuda, S., Sui, L., Tomczak, M., Veronig, A.L., Vlahos, L., White, S.M.: 2008, *Astron. Astrophys. Rev.* **16**, 155.
Lario, D., Sanahuja, B., Heras, A.M.: 1998, *Astrophys. J.* **509**, 415.
Lecacheux, A.: 2000, In: *Radio Astronomy at Long Wavelengths*, *Geophys. Monogr. Ser.* **119**, AGU, Washington, 312.
Lin, R.P., Anderson, K.A., Ashford, S., Carlson, C., Curtis, D., Ergun, R., Larson, D., McFadden, J., McCarthy, M., Parks, G.K., Rème, H., Bosqued, J.M., Coutelier, J., Cotin, F., D'Uston, C., Wenzel, K.-P., Sanderson, T.R., Henrion, J., Ronnet, J.C., Paschmann, G.: 1995, *Space Sci. Rev.* **71**, 125.
Lin, R.P., Dennis, B.R., Hurford, G.J., Smith, D.M., Zehnder, A., Harvey, P.R., Curtis, D.W., Pankow, D., Turin, P., Bester, M., *et al.*: 2002, *Solar Phys.* **210**, 3.
Lintunen, J., Vainio, R.: 2004, *Astron. Astrophys.* **420**, 343.
Maia, D.J.F., Gama, R., Mercier, C., Pick, M., Kerdraon, A., Karlický, M.: 2007, *Astrophys. J.* **660**, 974.
Malandraki, O.E., Sarris, E.T., Lanzerotti, L.J., Trochoutsos, P., Tsiropoula, G., Pick, M.: 2002, *J. Atmos. Solar-Terr. Phys.* **64**, 517.

McComas, D.J., Bame, S.J., Barker, P., Feldman, W.C., Phillips, J.L., Riley, P., Griffe, J.W.: 1998, *Space Sci. Rev.* **86**, 563.

Müller-Mellin, R., Kunow, H., Fleißner, V., Pehlke, E., Rode, E., Röschmann, N., Scharmberg, C., Sierks, H., Rusznyak, P., McKenna-Lawlor, S., Elendt, I., Sequeiros, J., Meziat, D., Sanchez, S., Medina, J., Del Peral, L., Witte, M., Marsden, R., Henrion, J.: 1995, *Solar Phys.* **162**, 483.

Palmer, I.D.: 1982, *Rev. Geophys. Space Phys.* **20**, 335.

Reames, D.V.: 1999, *Space Sci. Rev.* **90**, 413.

Reames, D.V.: 2009, *Astrophys. J.* **693**, 812.

Roelof, E.C.: 1969, In: Ögelman, H., Wayland, J.R. (eds.) *Lectures in High-Energy Astrophysics,* NASA **SP-199**, 111.

Ruffolo, D.: 1995, *Astrophys. J.* **442**, 861.

Ruffolo, D., Khumlumlert, T., Youngdee, W.: 1998, *J. Geophys. Res.* **103**, 20591.

Saiz, A., Evenson, P., Ruffolo, D., Bieber, J.W.: 2005, *Astrophys. J.* **626**, 1131.

Stone, E.C., Frandsen, A.M., Mewaldt, R.A., Christian, E.R., Margolies, D., Ormes, J.F., Snow, F.: 1998, *Space Sci. Rev.* **86**, 1.

Torsti, E.C., Valtonen, E., Lumme, M., Peltonen, P., Eronen, T., Luohola, M., Riihonen, E., Schultz, G., Teittinen, M., Ahola, K., Holmlund, C., Kelhä, V., Leppälä, K., Ruuska, P., Strömmer, E.: 1995, *Solar Phys.* **162**, 505.

Vainio, R., Valtonen, E., Heber, B., Malandraki, O.E., Papaioannou, A., Klein, K.L., Afanasiev, A., Agueda, N., Aurass, H., Battarbee, M., *et al.*: 2012, *J. Space Weather Space Clim.*, submitted.

Valtonen, E., Peltonen, J., Peltonen, P., Eronen, T., Hoisko, E., Louhola, M., Lumme, M., Nieminen, A., Riihonen, E., Teittinen, *et al.*: 1997, *Nucl. Instrum. Methods Phys. Res. A* **391**, 249.